Journal of Membrane Science 495 (2015) 198–205

Contents lists available at ScienceDirect

Journal of Membrane Science

journal homepage: www.elsevier.com/locate/memsci

On the analysis of FO mass transfer resistances via CFD analysis and film theory

Abraham Sagiv [a], Panagiotis D. Christofides [b], Yoram Cohen [b], Raphael Semiat [a,*]

[a] Wolfson Faculty of Chemical Engineering, Technion – Israel Institute of Technology, Technion City, Haifa 32000, Israel
[b] Department of Chemical and Biomolecular Engineering, University of California, Los Angeles, CA, USA

ARTICLE INFO

Article history:
Received 17 February 2015
Received in revised form
28 July 2015
Accepted 10 August 2015
Available online 11 August 2015

Keywords:
Forward Osmosis
Reverse Osmosis
Modeling
Concentration polarization
Desalination

ABSTRACT

The use of 2D finite element CFD model and the common film model (FM) for analysis of FO performance data was examined to assess the merits of conclusions derived from the above approaches regarding characterization of membrane and support layer resistances to water and salt permeation. The FM model leads to estimation of porous layer resistivity (K) that implies tortuosity/porosity ratio that is significantly higher than is physically attainable for typical membrane porous supports. Comparative FO data analysis with the 2D CFD model and FM approximation reveals that the latter approach overestimates (by an order of magnitude and greater) the significance of the permeation resistance of the FO membrane support layer. It is also shown that membrane (water and solute) permeabilities extracted from FO operation in the RO mode (FO/RO) are significantly higher than obtained from direct analysis of FO performance data via detailed 2D CFD modeling. The present analysis suggests that improvements in FO water permeability are more likely to emerge from developing higher permeability membrane skin and improved channel hydrodynamics (to decrease external concentration polarization) rather than from more permeable and thinner membrane support layer as has been asserted in various studies.

1. Introduction

In recent years there has been a growing interest in forward osmosis (FO) desalination [1] and the related area of pressure retarded osmosis (PRO) [2,3]. These operations have been made possible with the advent of semi-permeable polymeric membranes dating back to the early work in the late 1950s [4]. Experimental studies on the operational mechanisms of FO and PRO have focused primarily on process performance analysis, via the Film Model (FM) [1,2,5] with additional insight provided via two-dimensional (2D) numerical models [6–9]. The FM approach provides expressions for water and solute fluxes across the FO membrane based on one-dimensional diffusion–convection equation, assuming fully developed concentration and flow fields in the axial direction [10]. Using the FM approach, major efforts have been devoted to quantify the mass transfer resistance in the external layers (feed and draw side) relative to that of the membrane porous support layer [11].

Determination of the resistances to water permeation [12] in FO membrane systems, and thus the level of concentration polarization on both the feed and the draw sides, requires determination of the corresponding mass transfer coefficients k_f and k_d for the feed and draw sides of the membrane, respectively. The mass transfer coefficients are typically estimated from suitable empirical Sherwood Number correlations [11] or via the classical analytical Lévêque solution [13,14]. The majority of experimental FO studies have resorted to determining the membrane water permeability based on water permeation studies in the RO operational mode (i.e., under a measurable feed-side pressure) with pure water on both sides of the channel [2,15–17]. Salt transport coefficients have been similarly determined via FM analysis [2,15,16] from experimental data obtained from operation in the RO mode, with the target solute present in the channel feed side, Based on the above FM analysis approach, FO studies have typically reported membrane water permeability (A) and salt (B) transport parameters (along with the FO film model, to calculate the support layer resistivity constant K ($=t_s\tau/\varepsilon D$, where t_s, τ and ε are the thickness, tortuosity and porosity of the porous support and D is the solute diffusivity) [5,18]. Given K values as determined by the above FM/RO approach, FO studies typically report a structural parameter for the support layer defined as $S = t_s\tau/\varepsilon$. Studies that followed the above FM/RO approach, for analysis of experimental FO data, have concluded that internal concentration polarization (ICP) in the support layer is the dominant resistance to mass transfer that reduces the osmotic pressure driving force for water permeation across the FO membrane [19,20,5,12]. These

* Corresponding author. Fax: +972 4829 2009.
E-mail address: cesemiat@tx.technion.ac.il (R. Semiat).

http://dx.doi.org/10.1016/j.memsci.2015.08.022
0376-7388/

studies have encouraged efforts to develop membrane substrates of lower resistivity suggesting needed reduction of both the porous layer thickness and its porosity [12].

It is interesting to note that in order to force agreement of conclusions from CFD analysis results with FM/FO analysis, regarding the dominance of ICP over ECP, an unusually (or "unrealistically") thick support layer (up to a factor of 10 above typical support layer thicknesses) was assumed in certain CFD studies [7,8]. It is emphasized, however, that the majority of CFD studies have not considered the porous layer as a separate domain, but instead accounted for it through a flux boundary condition that combines with the film model [8]. In contrast, FO CFD models [7] that accounted for the detailed transport (fluid and solute) within the porous layer (of expected values of support layer tortuosity and porosity), and with solute concentration-dependent membrane permeability parameters extracted directly from FO experimental data, have shown conclusively that the ICP (i.e., associated with the support layer) contribution to the water overall permeation resistance is about an order of magnitude lower than the ECP contribution. It is also of interest to note that recent FM [12] and CFD [7,9] modeling of FO performance questioned the often reported dominance of the contribution of the ICP over the ECP.

There is significant differences in the published literature with respect to interpretation of experimental FO data regarding the significance of ICP relative to ECP. However, a quantitative explanation is yet to be advanced regarding the discrepancy between FM and CFD modeling studies regarding the significance of ICP. These discrepancies regarding the importance of ICP relative to ECP in FO operation have major relevance to directing future developments in FO. Accordingly, the present contribution focuses on comparison of CFD and FM analyses and the underlying assumptions and approximations inherent in the above approaches with the objectives of: (a) evaluating the validity of the commonly invoked assumption of concentration-invariant membrane transport coefficients, and (b) assessing the contribution of ICP relative to ECP to the total (including membrane, ICP and ECP layers) water permeation resistance.

2. Analysis of ICP and ECP in Forward Osmosis

2.1. Overview of workflow

In order to elucidate the relative contributions of ICP and ECP to the overall water permeation resistance in FO desalination, detailed analysis was carried out using recent comprehensive FO experimental datasets [2,15–17]. In the experimental FO system (Fig. 1) the membrane skin (thick line) faced the feed (*SFF* mode) and the porous support layer (*ps*) faced the draw solution. The feed and draw channels [15] were each 77 mm long, 26 mm wide, 3 mm in height, and with membrane support layer thickness of 0.05 mm. The feed and draw solution were DI water and aqueous NaCl solution (1–4 M), respectively, with the above two streams flowing co-currently at a crossflow velocity of 21.4 cm/s. The ICP and ECP in the above system were quantified via fully-coupled 2D CFD model simulations described in [9] and compared with results from the approximate film model [15]. In applying the CFD model, the draw solute concentration-dependent membrane water permeability (A) and salt transport coefficient (B) were extracted directly from the reported experimental water and salt flux data of [15; Fig. 2] following the approach described in [7].

The osmotic pressure driving force across the membrane active layer is governed by salt and draw solute concentrations at the membrane surface in the feed and draw channel sides. As a consequence of ECP (in feed and draw channels) and (dilutive) ICP in

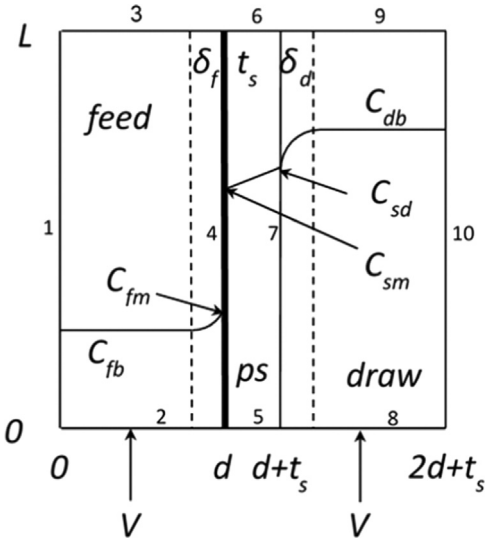

Fig. 1. Schematic representation of the FO unit used in the present analysis. System dimensions and flow conditions (Tables 2, 3 of [7]) are as reported in Fig. 2 of [11]. The skin (thick line) faces the feed channel (*SFF* mode) and the porous support layer (*ps*) faces the draw channel with both the feed and draw solutions in co-current flow. Nomenclature: *C*-concentration, *d*- feed or draw channel thickness, δ–concentration polarization thickness, *L*-membrane length, *ps*–porous support, *V*-crossflow velocity. Subscripts: *b*-bulk, *d*-draw, *f*-feed, *m*-membrane.

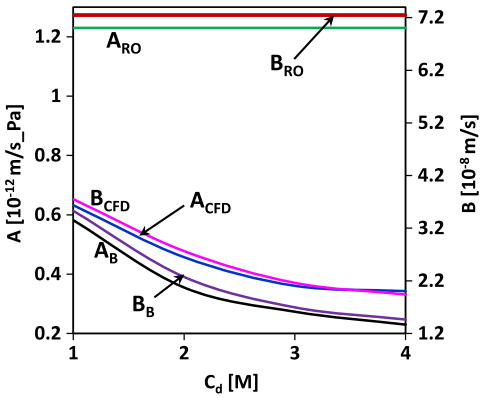

Fig. 2. Membrane water permeability (A) and salt transport parameter (B) extracted from the FO data (DI water feed and NaCl draw solution) in Fig. 2 of [15a] Tables 2 and 3 of [11a] via matching of the reported experimental and CFD model calculated water and salt fluxes. Indices RO, CFD and B denote A and B derived from RO experiments, the current CFD 2D model and based on the bulk osmotic pressure and concentration driving forces, respectively.

the porous layer, the actual osmotic pressure driving force across the membrane and the porous layer is lower than the overall driving force in terms of the bulk osmotic pressure difference (i.e., $\pi_{db} - \pi_{fb}$, Fig. 1). One can define the overall resistance to water permeation (R_T), based on the overall bulk osmotic pressure difference, such that the permeation flux in terms of the individual resistances can be expressed as,

$$J_w = (\pi_{db} - \pi_{fb})/R_T = (\pi_{db} - \pi_{pd})/R_d = (\pi_{pd} - \pi_{pm})/R_p = (\pi_{pm} - \pi_{fm})/R_m = (\pi_{fm} - \pi_{fb})/R_f \quad (1)$$

in which $R_T = R_d + R_p + R_m + R_f$, where the percent contribution of each of the domains to the overall permeation resistance can be calculated (i.e., $[R_i/R_T] \times 100$) from knowledge of the solute concentration. Here it is noted that for FO studies in which the feed-side is a salt-free solution as in [15] the resistance to water transport on the feed-side is identically zero; this implies that $\pi_{fm} = \pi_{fb}$ and thus only three resistances need to be considered for

the above case, namely, R_d, R_p and R_m.

2.2. The CFD model

The finite element (FEM) 2D CFD model for FO operation in SFF mode followed the formulation described in [9]. Briefly, the steady-state cross flow of the solutions along the feed and draw channels of the FO unit is governed by Navier–Stokes equations

$$\rho_i(\boldsymbol{u_i}\cdot\nabla)\boldsymbol{u_i} = \nabla\cdot\left[-p_i\mathbf{I} + \eta_i\nabla\boldsymbol{u_i}\right],\ \nabla\cdot\boldsymbol{u_i} = 0 \tag{2}$$

in which the index i in Eq. (2) is replaced by either f for the feed channel or d for the draw channel, ρ is the solution density, η is dynamic viscosity, p is pressure, and the 2D velocity vector is denoted by $\boldsymbol{u}=(v, u)$, where v and u are in the axial and traverse flow directions, respectively. The flow of the salt (NaCl) solution through the porous support is governed by the Brinkman equation [21]

$$\frac{\eta_p}{\kappa}\boldsymbol{u_p} = \nabla\cdot\left[-p_p\mathbf{I} + \frac{\eta_p}{\varepsilon_p}\nabla\boldsymbol{u_p}\right],\ \nabla\cdot\boldsymbol{u_p} = 0 \tag{3}$$

in which η_p the dynamic viscosity [Pa s], κ [m^2] is the solution permeability and ε_p is the porosity of the support layer. Solute diffusion in the different domains (Fig. 1) of the FO channels is described by the convection–diffusion equation,

$$\nabla\cdot(D_i\nabla c_i) = \boldsymbol{u_i}\cdot\nabla c_i \tag{4}$$

where D_i is the solute diffusion coefficient in the solution phase, which in the support layer (denoted by subscript p) is determined from $(D_i)_p=\varepsilon D/\tau$. The water flux, J_w, across the membrane skin is given by [6]

$$J_w = A(\pi_{p,m} - \pi_{f,m}) \tag{5}$$

in which $\pi_{p,m}$ and $\pi_{f,m}$ are the osmotic pressures at the membrane surface (denoted by subscript m) interface with the porous layer (subscript p) and feed (subscript f) solution, respectively. Finally, solute flux across the active membrane is typically expressed by [6]

$$J_s = B(c_{p,m} - c_{f,m}) \tag{6}$$

Eqs. (2–6), describe the hydrodynamics and solute diffusion in the various domains of the FO membrane channel system (Fig. 1) with solution (η, ρ, π), solute (D) and membrane (A and B) parameters that can in principle vary with concentration. In the present analysis, the membrane transport parameters (A and B) were extracted from FO experimental data reported in [15] using the CFD model [Eqs. (2–6)] over the range of reported draw solute concentrations. The above was accomplished by matching the experimental water and salt fluxes with the CFD model predictions. The coupled CFD model equations were solved via the finite-element method with a sufficient degree of mesh density for the feed, draw and support layer established following [9] so as to ensure grid-independent solution (Table 1).

2.3. The film model for FO transport analysis

According to the film model, which assumes fully developed flow and concentration fields, and based on the classical flux expressions [Eqs. (5) and (6)], the water and salt fluxes (J_w, and J_s, respectively), considering mass transfer resistance in the different membrane channel domains (i.e., feed, draw, support layer and active membrane skin) are given by [11,12],

$$J_w = \frac{K_m k_f k_d}{K_m k_f + K_m k_d + k_f k_d}\ln\left[\frac{A\pi_d + B}{A\pi_f + B + J_w\exp(-J_w/k_f)}\right] \tag{7}$$

Table 1
Boundary condition settings for the FO system described in Fig. 1 and Eqs. (2–6).

BC[a] no.	NS feed[a]	CD feed[a]	Brinkman support[a]	CD support	NS draw	CD draw
1	Wall	No flux				
2	Inlet v_{f0}	Conc. c_{f0}				
3	Outlet $p=0$	Outflow				
4	Outlet J_w	Inward J_s	Inlet J_w	Zero inward flux		
5			Wall	No flux		
6			Wall	No flux		
7			Outlet $p=0$	$c_p=c_d$	Inlet J_w	$c_d=c_p$
8					Inlet v_{d0}	Inlet c_{d0}
9					Outlet	Outflow
10					Wall	No flux

[a] BC= boundary condition, NS=Navier-Stokes equations, CD= convection and diffusion equations, Brinkman = Eq. (3); Feed and draw inlet cross flow velocities are respectively, v_{f0} and v_{d0}; Feed and draw inlet concentrations are respectively, c_{f0} and c_{d0}; Pressure is denoted by p; Indices f, p, d and 0 respectively are for feed, porous support, draw and given data.

$$J_s/B = \frac{C_{db} + J_s/J_w}{\exp(J_w/K_m)\exp(J_w/k_d)} - (C_{fb} + J_s/J_w)\exp(J_w/k_f) \tag{8}$$

in which K_m is the reciprocal of the support layer resistivity K, and where the feed and draw-sides mass transfer coefficients (k_f and k_d, respectively) are generally estimated using suitable mass transfer correlation [18,13], but typically resort to estimations obtained from the analytical Lévêque solution [13],

$$k = 1.85\frac{D}{d_h}\left(Re\cdot Sc\frac{d_h}{L}\right)^{1/3} \tag{9}$$

in which $Sc = \nu/D$ is the solute Schmidt number, and d_h, L and Re are the channel (feed or draw) hydraulic diameter, length, and Re number, respectively. It can be shown, based on the classical description of diffusion in a porous layer and the film model, that the support layer resistivity K (often expressed as the inverse of the mass transfer coefficient (K_m) for the support layer, known as the), can be determined from [18]

$$K \equiv \frac{1}{K_m} = \frac{1}{J_w}\ln\left(\frac{B + A\,\pi_{d,b}}{A\pi_{fm} + B + J_w}\right) \tag{10}$$

It is noted that in FO experiments in which freshwater is used the term containing the osmotic pressure (π_{fm}) in Eq. (10) can be neglected.

The solute concentrations at the membrane surface in the feed (C_{fm}) and support (C_{pm}) sides and at the porous support-draw solution interface (C_{pd}) are given by [11]

$$C_{fm} = (C_{fb} + J_s/J_w)\cdot\exp\left(\frac{J_w}{k_f}\right) - J_s/J_w \tag{11}$$

$$C_{p\,d} = \frac{(C_{db} + J_s/J_w)}{\exp\left(\frac{J_w}{k_d}\right)} - J_s/J_w \tag{12}$$

$$C_{pm} = \frac{(C_p + J_s/J_w)}{\exp(J_w\cdot K)} - J_s/J_w \tag{13}$$

It is noted that the derivation of the above FM model equations (Eqs (11–13)) assumes all transport parameters to be concentration-independent [5,15,18]. Moreover, it has been common in FO studies to rely on membrane water permeability (A) and salt transport coefficient (B) that are derived from experiments in the RO operational mode (i.e., FO/RO approach) where hydraulic

pressure is the driving force for water permeation [18]. In such experiments, FO membrane water permeability is typically accomplished with DI water in both the feed and draw sides. In RO experiments from which the solute transport parameter B is determined, water and solute flux are in the same direction; however, in FO operation the draw solute flux is in the opposite direction to the water flux. Impact of the above on water flux has been debated in the literature [15,18,7] but not resolved. Notwithstanding the current debate, it is stressed that experimental water flux data from available FO studies (e.g., [7] and [15]) clearly show the variability of the water permeability and transport coefficient with respect to the inlet draw solution concentration; Such a trend is observed even when these coefficients are calculated based on the bulk osmotic pressure driving force (i.e., $A_b=J_w/\Delta\pi_b$ and $B_b=J_s/\Delta C_b$, in which $\Delta\pi_b$ and ΔC_b are the osmotic pressure and concentration driving forces based on the bulk solutes concentration, respectively).

Given FM based estimates of the support layer parameter K for various membranes and in different plate-and-frame type experimental systems, numerous FO studies have argued that the overall resistance to water permeation can be reduced by increasing the porosity and decreasing the thickness and potentially the tortuosity of the membrane support layer [19,5,12]. In order to evaluate the above assertions, it is instructive to note first that the ratio λ of the tortuosity τ to porosity ε of the support layer is related to the commonly reported support layer resistivity (K) as given below [11]

$$\lambda = \frac{\tau}{\varepsilon} = K\frac{D}{t_s} \tag{14}$$

Accordingly, the validity of reported K values, as calculated, based on the film model (Eq. (10)), can be ascertained by checking that the ratio λ is within physically realistic bounds. For example, review of the literature suggests that [7,22,23] the tortuosity and porosity of porous supports (as for porous materials in general) are expected to be in the range of 1.2–1.7 and 0.35–0.77, respectively, which leads to λ values in the range of 1.56–4.86; note that the minimum τ value is unity and the range of ε is [0–1]. Therefore, as discussed in Section 3, any estimates of K that significantly deviate from the above λ range should be questionable and suggest unreliability of the presented conclusions regarding the relative contributions of ECP and ICP to the total FO water permeation resistance.

2.4. Analysis of the contributions of feed and draw channel ECP and porous layer ICP to the overall water permeation resistance and the porous layer structural parameter

The relative significance of ECP and ICP was explored via an illustrative test case based on analysis of available FO performance data that includes both water and solute fluxes [15]. The concentration driving forces at each of the different domain interfaces (traverse to the membrane surface) were determined via both CFD analysis and the commonly used film model approximation (Section 3.2). The concentration fields obtained from CFD analysis were determined for the experimental system of [15] using the best fit membrane transport coefficients (A and B). These coefficients were determined by matching the experimental water and salt fluxes with the CFD model results as per the approach described in [7]. The relative significance of ECP and ICP, as determined from the FO data, was expressed in terms of the resistances to water permeation apportioned to the various domains (Fig. 1) based on:

(1) CFD model; and

(2) FM approximation (Section 3.2) whereby the A and B parameters were those extracted as concentration-dependent coefficients (Appendix A) based on CFD analysis (FM/ CFD approach) of FO performance data in [15], or on the basis of experimental data in the RO operational mode (i.e., FM/RO approach).

In carrying out the CFD simulations, the porous support layer parameters τ and ε were taken to be in the ranges of 1.2–1.7 and 0.35–0.77, respectively, which are expected for membrane support layers [7,22,23]. The tortuosity/porosity ratio corresponding to the above is $1.56 < \lambda = \tau/\varepsilon < 4.86$. It is noted that over the above range of λ uncertainty in the extracted membrane A_{CFD} and B_{CFD} parameters was no higher than 2.5–2.7% indicating that ICP did not dominate the overall resistance as further discussed in Section 3. The FM/CFD and FM/RO analyses approaches were then compared with respect to the estimated support layer resistivity K values in relation to the physical bounds on tortuosity/porosity ($\lambda = \tau/\varepsilon$). Finally, evaluation of K and λ was also carried out based on the FM approximation with A and B estimated based on the feed draw and salt feed concentrations (termed here FM/B approach) which for the low recovery FO experiments in [15] approximate the bulk concentrations.

3. Results and discussion

3.1. Membrane permeability coefficients (A and B) extracted from experimental data via FM and CFD analyses

In order to present the prevailing issues with respect to extraction of membrane transport coefficients from experimental data, the FO dataset in [15] (aqueous NaCl draw solute inlet concentration range of 1–4 M; Section 2.1) was selected as an illustrative example. The dataset was first analyzed to extract the membrane (active layer; Fig. 1) A and B coefficients (denoted as A_{CFD} and B_{CFD}) using the present CFD model (Section 2.4). Both of the above coefficients declined in magnitude with increasing draw solute concentration (Fig. 2) consistent with previous work [7] with different draw solutes (NaCl, KCl and NH_4HCO_3).

In the present case, A and B extracted from the data set of [15] decreased by about 46% and 48%, respectively, as the draw solute (NaCl) concentration increased from 1 M to 4 M. The A and B values were not significantly impacted by the support layer tortuosity/porosity ratio [i.e., λ, Eq. (14)], demonstrating only 6% and 8% variation, respectively, even when λ was varied over a significant range of 1.56–4.86] suggested in previous studies [7,22,23]. It is noted that the A and B parameter values for the HTI-CTA membrane were reported in [15], based on RO permeation experiments, as constants being 1.23×10^{-12} m/(s Pa) and 7.25×10^{-8} m/s, respectively; these values were higher by factors of 1.99 and 1.94, respectively, than the highest values determined by CFD analysis of the same dataset (Fig. 2). It is interesting to note that approximation of the A and B parameters based on bulk concentrations (i.e., C_{fb} and C_{db}) also leads to a clear trend of values that decrease with increasing draw solute concentration; even this approximation, results in A and B transport parameters that much closer (relative to the FM/RO analysis) to the intrinsic values determined based on CFD analysis (Table 2).

In order to assess if the magnitudes of A and B as derived from FO-RO approach are suitable for FO process analysis, it is instructive to compare the support layer tortuosity/porosity ratio (i.e., $\lambda = \tau/\varepsilon$) obtained based on the various analyses approaches (Table 2). Accordingly, based on the reported FO data of [15], λ was calculated from Eq. (14) whereby the support resistivity K was determined from its FO film model expression (i.e., Eq. (10)) and

Table 2
Comparison of K and τ/ε values derived from Eqs. (10) and (14) based on three different approaches to estimating the membrane A and B parameters using experimental FO water and draw solute flux data reported in [15].

C_d	J_w	K [10^5 s/m]			$\lambda = \tau/\varepsilon$		
[M]	[μm/s]	FM/RO[a]	FM/B[b]	FM/CFD[c]	FM/RO	FM/B	FM/CFD
1	2.75	2.75	1.01	0.526	9.85	3.61	1.88
2	3.74	3.26	1.07	0.702	11.7	3.82	2.51
3	4.72	3.13	1.13	0.512	11.2	4.03	1.83
4	5.66	2.93	1.18	0.626	10.5	4.22	2.24

[a] Based on Eq. (13), with A and B coefficients reported in [15] based on permeation experiments in RO operational mode (FM/RO approach, Section 2.4): $A=1.23\times10^{-12}$ m/(s Pa) and $B=7.25\times10^{-8}$ m/s.
[b] Based on the FM equations as in (a) with A and B coefficients derived from the flux definitions of Eqs. (5), (6), (11)–(13) where the driving force is based on the bulk concentrations (i.e., FM/B approach, Section 2.4).
[c] Based on the FM equations as in (a) with A and B coefficients derived from the CFD model (FM/CFD approach, Section 2.4, Appendix A). The ranges of A_{CFD} and B_{CFD} in Appendix A are respectively (0.618–0.335) x10^{-12} m/(s Pa) and (3.727–1.954) x10^{-8} m/s for C_d=1–4 M.

using the membrane A and B transport parameters as determined based on the FM/RO, FM/CFD and FM/B approaches (Section 2.4). The results shown in Table 2 indicate that the support layer resistivity (i.e., K) values (for the FO data reported in [15]) are in the range of 2.75–3.26 which is about a factor of 2.5–3 and 4.7–5.2 higher than obtained by the FM/B and FM/CFD approaches, respectively. Based on the K values as determined based on the FM/RO approach, the attained $\lambda(=\tau/\varepsilon)$ range of 9.85-11.7 is unrealistic as it is significantly higher than the physically attainable range of 2.3–4.7 for practical membrane supports for which $\varepsilon = 0.5 - 0.74$ and $\tau = 1.7 - 2.35$, [24]. The λ range of 3.61–4.22 based on the FM/B approach is also significantly above the expected physically meaningful range. In contrast, the FM/CFD approach leads to λ range of 1.83–2.51which is closer to that expected for porous supports. The different λ ranges were ascertained given the range of A's and B's given in Fig. 2 using Eqs. (10) and (14). The above analysis suggests that the practiced approach of utilizing A and B parameters derived from RO experiments (i.e., FM/RO, Section 2.4) is inappropriate for FO analysis as it would imply accepting physically unrealistic porous support porosity and/or tortuosity values. On the other hand, using A and B values based on the CFD model (FM/CFD approach) results in realistic τ/ε ratio suggesting that the film model can provide a reasonable approximation of FO performance, provided that the proper membrane transport parameter values are utilized.

It is tempting to argue that the CFD analysis may be biased since the support domain is modeled directly using reasonable values of the support layer porosity and tortuosity [7,22,23]. However, as shown in the present work, the extracted membrane A and B parameters were only marginally sensitive to the porous support layer porosity, tortuosity and thickness over a wide range of physically realizable values for these parameters (Section 2.4). Moreover, it is important to recognize that CFD follows a fundamental description of the structure of the support layer consistent with the rich body of knowledge regarding transport in porous media [21]. Improved, albeit approximate A and B values may be obtained based on bulk concentration driving forces (Fig. 2), but ultimately the most accurate approach is to extract the values from CFD model analysis.

3.2. Mass transfer resistance of the various FO domains

Numerous FO studies have argued, relying on the crude FM/RO approximation (Section 2.4, [15,7]), that the major resistance to water permeation is due to the support layer (i.e., due to ICP). Assessment of the relative significance of the resistances to water transport across the different membrane channel domains (i.e., R_f, R_d, R_s and R_m for the feed, draw, support layer and active membrane domains, respectively), irrespective of the transport model used (e.g., FM approximation or detailed spatial CFD modeling), requires the relevant membrane water permeability and salt transport coefficient. Therefore, here we revisit the question of the significance of the support layer ICP relative to ECP, using the detailed FO data of [15] as a test case. Accordingly, the water permeation resistances are quantified based on: (a) direct CFD analysis of experimental FO data (Section 3.1, Appendix A), and (b) FM approximation with CFD derived membrane transport parameters [7] (i.e., FM/CFD approach, Section 2.2, Appendix A). The resulting percent contributions of the membrane, support layer and draw channel resistances (R_s and R_d) to the total FO resistance to water permeation, as per the CFD and FM/CFD approaches, as well as per the FM analysis reported in Fig. 3 of [15], are provided in Table 3 for the FO experiments of [15] with pure water feed and draw solution. It is noted that since pure water was the feed in the study of [15], the feed-side resistance (R_f) vanishes.

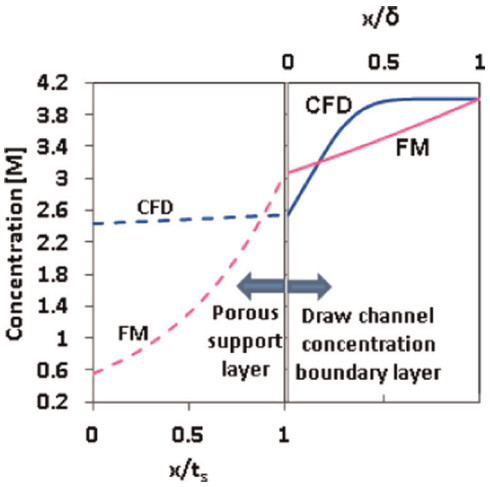

Fig. 3. Comparison of concentration profiles within the support layer and draw side concentration boundary layer for the case of C_{fb}=0 and C_{db}=4 M (NaCl) for the mid-section of a 7.7 cm long FO membrane channel of [15]. In the porous support layer the distance from the membrane skin is non-dimensionalized with respect to the support layer thickness (i.e., x/δ; $\delta=\delta_s$=50 μm). In the draw channel side, the distance from the active membrane surface is non-dimensionalized with respect to the draw solute boundary layer thickness ($\delta=\delta_d$ =81 μm as determined in the film models and $\delta=\delta_d$=296 μm based on the CFD model numerical solution).

Table 3
Contributions of membrane, support layer and draw-side to the overall water permeation resistance determined based on the CFD, FM/RO and FM/CFD approaches[a].

Data in Fig. 2 of [15], FM % drop in Fig. 3 of [11], ***ε/ τ=0.75/1.2*** *[23]*

C_d, M	*Membrane resistance, R_m (%)*			*Support layer resistance, R_s (%)*			*Draw-side resistance, R_d (%)*		
	FM/RO[b]	FM/CFD[c]	CFD[c]	FM/RO	FM/CFD	CFD	FM/RO	FM/CFD	CFD
1	41.7	76.6	86.9	46.8	11.3	1.27	11.3	11.7	11.8
2	29.2	69.9	82.0	55.0	14.2	1.68	15.6	15.8	16.4
3	21.8	63.8	79.3	59.2	16.7	1.89	19.0	19.4	18.9
4	19.1	58.3	75.0	60.4	18.8	2.20	20.4	22.8	22.9

[a] Section 2.4.
[b] support layer resistivity (i.e., K) values obtained from the data of [15] (Table 2).
[c] A and b parameters obtained from CFD analysis (Fig. 2).

However, one would expect, based on previous CFD and FM analyses [7], that for a saline feed-side solution the contribution of the feed-side concentration boundary layer to the overall resistance would be at a level similar to the draw-side (under conditions of similar hydrodynamics for channels of similar geometry and cross flow velocities). The percent contributions of the draw-side (R_d) and support layer (R_s) to water permeation resistance increases with increasing draw solute feed concentration, while the membrane resistance (R_m) correspondingly decreases. However, the FM/RO analysis suggests unrealistically high R_s (~47–60% of R_T) compared to the CFD model results that reveal R_s being ~1.3–2.2% of R_T. Based on the FM/CFD approach (i.e., with CFD derived A and B coefficients; Sections 2.4 and 3.1) R_s is in the range of 11–19% of R_T which, although a factor of 3–4 lower than for the FM/RO approach, is still nearly an order of magnitude higher than predicted by CFD analysis. The FM/RO analysis (and even the somewhat improved FM/CFD approach) leads to the erroneous conclusion that the support layer resistance to water permeation is dominant over both the membrane and draw-side resistances. The above conclusion is the result of significant overestimates of the membrane A and B coefficients by the FM/RO approach that effectively materializes in a magnitude of the porous layer τ/ε ratio that is physically unrealizable for porous supports. Moreover, even with more accurate A and B parameters obtained from CFD analysis, one must recognize that the film model (i.e., FM/CFD approach) is an approximation as is evident from comparison of the concentration profiles shown in Section 3.3. It is unfortunate that there has been a significant perpetuation of FO analysis that is based on characterization of FO membrane transport coefficients from the film model and experiments in the RO operational mode. The present analysis clearly reveals that the ICP layer resistance is not dominant over ECP, a conclusion that is contrary to the prevailing thought in the published FO literature.

3.3. Concentration profiles across the support and the draw boundary layers

The differences between predictions of the importance of the different FO domains to the overall resistance to water permeation can be illustrated by comparing the solute concentration profiles obtained from the FM and CFD models. The concentration profiles for the solute in the porous support ($C_p(x)$) and draw side ($C_d(x)$) as obtained from the film model can be expressed as [11],

$$C_p(x) = -\frac{J_s}{J_w} + \left(C_{pm} + \frac{J_s}{J_w}\right)\exp(J_w K \cdot x), \quad 1 \geq x = \frac{x'}{t_s} \geq 0 \tag{15}$$

$$C_d(x) = -\frac{J_s}{J_w} + \left(C_{pd} + \frac{J_s}{J_w}\right)\exp\left(\frac{J_w}{k_D}x\right), \quad 1 \geq x = \frac{x'}{\delta_D} \geq 0 \tag{16}$$

in which x and x' are the normalized distances from t_s=50 μm [15] and $\delta_{D\text{-}FM}$=81 μm [15] and $\delta_{D\text{-}CFD}$=296 μm, respectively. For convenience of plotting the concentration profiles, the normalization length scales for the porous support and draw channels were taken as the thicknesses of the support (t_s) and the draw channel-side concentration boundary layer (δ_D), respectively. It is noted that for at x=1 Eqs. (15) and (16) reduces to Eqs. (12) and (13) (Section 2.3), respectively, reported in [11]. An illustration of the differences in the draw solute concentrations is provided in Fig. 3, based on the data in [15], for a NaCl draw solute concentration of 4 M at the mid-section of the 7.7 cm channel. It is apparent that the FM model with the RO-derived A and B membrane parameters (FM/RO approach, Section 2.4) predicts dramatic draw solute concentration reduction (by a factor of ~4) at the membrane-support layer interface (C_{pm}) relative to the concentration at the edge of the concentration boundary layer in the draw channel. Moreover, a thinner draw channel concentration boundary layer (by a factor of ~3.6) is predicted by the CFD relative to the FM model. It is also noted that the approximate film model yields nearly linear profiles for the two relatively thin porous support and draw channel concentration boundary layer. In contrast, the CFD draw solute concentration profiles in the draw and support layers are non-linear with the expected behavior of a concentration that asymptotically approaches the bulk concentration in the draw channel within a realistic concentration boundary layer thickness. The above behavior indicates that erroneous conclusions regarding FO performance with respect to the role of mass transfer resistances in the different domains can result from use of the film model, particularly when one assumes membrane transport parameters (A and B) that are obtained from experiments in the RO permeation mode.

4. Conclusions

A comparative analysis of laboratory FO performance data via 2D finite element CFD and the commonly reported film model (FM) was carried out in order to clarify the relative significance of internal versus external concentration polarization in FO operation. Analysis of experimental FO data demonstrated that the main resistance to water permeation in FO operation is in fact due to the membrane skin, followed by contribution of the external concentration polarization in the feed and draw channels and lastly the membrane support layer. Here we note that various studies have reported porous layer resistivity (K) that implies tortuosity/porosity ratio that is a factor of ~2–5 higher than is physically realizable for typical porous supports. In closure, it is concluded that CFD model analysis of FO performance data suggests that efforts to improve FO flux would benefit more from: (a) membrane skins of improved permeability rather than thinner support layers of increased porosity, and (b) module design to improve channel hydrodynamics so as to reduce the ECP in both the draw and feed channels.

Acknowledgments

This research was supported by Grant no. 2014337 from the United States-Israel Binational Science Foundation (BSF). P. Christofides and Y. Cohen also acknowledge support from the California Department of Water Resources.

Appendix A. Extraction of membrane A and B transport coefficients via CFD analysis

Membrane intrinsic permeability coefficients for water (A) and salt (B) are needed for in order to quantitatively model FO transport behavior. Accordingly, the CFD model (Section 2.2) was utilized, whereby the transport coefficients A and B were extracted from the experimental water and salt flux data reported in Fig. 2 of [15] by matching the reported flux data with model predictions as described in Section 3.1 following the detailed approach in [7]. Parameters and experimental conditions for the simulations are listed in Tables 2 and 3 of [11]. FO supports porosity and tortuosity in the range of 0.60–0.75 and 1.7, respectively [7,25,26] have been reported in FO studies; thus, a reasonable mid-range of ε=0.56 and τ = 1. 7 was adopted. Support layer permeability was set at $\kappa = 2.34 \times 10^{-15}$ m^2, as per previous work [7]. Here it is noted that various simulations were carried out with different support layer porosity, permeability and tortuosity values (over a reasonable

range of these parameters as reported in various studies for porous supports; Section 3.1, [7]) in order to assess the parameter sensitivity of the CFD model calculations of A and B. These simulations revealed that the porous support layer (typically of thickness of the order of 50–500 μm [27], and 50 μm for the system of [15] analyzed in the present work) had a negligible impact on the predicted water flux and correspondingly also little impact on the values of the extracted A and B transport parameters (Sections 2.4 and 3.1). The above conclusion is consistent with the assertion that the support layer resistance to water permeation is marginal compared to the resistances offered by the membrane itself and due to external concentration polarization. Once the A and B coefficients were extracted from the experimental data (Fig. 2 of [15]) via the CFD model, the variability of these transport coefficients (designated here as A_{CFD} and B_{CFD}) with the draw solute feed concentration ($1M \le C_d \le 4M$) was expressed via the following correlations,

$$A_{CFD} = \left(0.886 - 0.293 \cdot C_d + 0.393 \cdot C_d^2\right) \cdot 10^{-12}, \quad [\mathrm{m/(s\ Pa)}] \tag{A1}$$

$$B_{CFD} = \left(5.12 - 1.56 \cdot C_d + 0.191 \cdot C_d^2\right) \cdot 10^{-8}, \quad [\mathrm{m/s}] \tag{A2}$$

The above correlations fitted the values of the extracted A and B values with a deviation of less than 3% and 1%, respectively. The above expressions for A and B were then utilized in the numerical CFD model to carry out the range of simulations as described in Section 3.

Nomenclature

A	water permeability coefficient [m/(s Pa)]
B	salt permeability coefficient [m/s]
C, c	concentration [M, mol/m^3]
D	diffusivity [m^2/s]
d	channel thickness [m]
d_h	hydraulic diameter [m]
I	identity matrix
J_s	salt flux across the membrane [mol/(m^2 s)]
J_w	water flux across the membrane [m/s]
K	support resistivity [s/m]
K_m	mass transfer coefficient in the support [Eqs. (10), 1/K, m/s]
k	mass transfer coefficient [m/s]
L	membrane length [m]
p	hydraulic pressure [Pa]
R	resistance [Pa s/m]
Re	Reynold number [dimensionless]
S	structural parameter [m]
Sc	Schmidt number [dimensionless]
t_s	support thickness [m]
u	x-direction component of the solution velocity [m/s]
V	cross-flow velocity [m/s]
v	y-direction component of the solution velocity [m/s]

Greek letters

∇	derivative operator
δ	concentration polarization thickness
ε	membrane porosity
η	dynamic viscosity [Pa s]
κ	solution permeability coefficient across the support layer [m^2]
λ	defined in Eq. (14) [dimensionless]
υ	kinematic viscosity [m^2/s]
π	osmotic pressure [Pa]
ρ	solution density [kg/m^3]
τ	membrane pore tortuosity

Subscripts

b	bulk
d	draw
CFD	of the current 2D finite element model
FM	of the Film model
f	feed
i	index
m	membrane
p	porous support
RO	of the Reverse Osmosis experiments
s	salt
T	total or overall
w	water

References

[1] S. Kimura, Analysis of reverse osmosis membrane behaviors in a long-term verification test, Desalination 100 (1995) 77–84.
[2] K.L. Lee, R.W. Baker, H.K. Lonsdale, Membranes for power generation by pressure-retarded osmosis, J. Membr. Sci. 8 (1981) 141–171.
[3] Y. Oh, S. Lee, M. Elimelech, S. Lee, S. Hong, Effect of hydraulic pressure and membrane orientation on water flux and reverse solute flux in pressure assisted osmosis, J. Membr. Sci. 465 (2014) 159–166.
[4] S.T. Yuster, S. Surirajan, K. Bernstein, Sea Water Demineralization by the Surface Skimming Process, University of California (UCLA), Dept. of Engineering, 1958, Rept. 58-26.
[5] G.T. Gray, J.R. McCutcheon, M. Elimelech, Internal concentration polarization in forward osmosis: role of membrane orientation, Desalination 197 (2006) 1–8.
[6] M.F. Gruber, C.J. Johnson, C.Y. Tang, M.H. Jensen, L. Yde, C. Helix-Nielsen, Computational fluid dynamics simulations of flow and concentration polarization in forward osmosis membrane systems, J. Membr. Sci. 379 (2011) 488–495.
[7] A. Sagiv, A. Zhu, P.D. Christofides, Y. Cohen, R. Semiat, Analysis of forward osmosis desalination via two-dimensional FEM model, J. Membr. Sci. 464 (2014) 161–172.
[8] M. Park, J.H. Kim, Numerical analysis of spacer impacts on forward osmosis (1910) 20.
[9] A. Sagiv, R. Semiat, Finite element analysis of forward osmosis process using NaCl solutions, J. Membr. Sci. 379 (2011) 86–96.
[10] C.H. Tan, H.Y. Ng, Modified models to predict flux behavior in forward osmosis in consideration of external and internal concentration polarizations, J. Membr. Sci. 324 (2008) 209–219.
[11] C. Suh, S. Lee, Modeling reverse draw solute flux in forward osmosis with external concentration polarization in both sides of the draw and feed solution, J. Membr. Sci. 427 (2013) 365–374.
[12] R.W. Field, J.J. Wu, Mass transfer limitations in forward osmosis: are some potential applications overhyped? Desalination 318 (2013) 118–124.
[13] M.D. Lévêque, Les lois de la transmission de chaleur par convection, Ann. Mines, Mem., Ser. 12 (13) (1928) 201.
[14] J. Zeman, A.L. Zydney, Macrofiltration and Ultrafiltration: Principles and Applications, Marcel Dekker (1996), p. 359.
[15] W.A. Phillip, J.S. Yong, M. Elimelech, Reverse draw solute permeation in forward osmosis: modeling and experiments, Environ. Sci. Technol. 44 (2010) 5170–5176.
[16] T.Y. Cath, M. Elimelech, J.R. McCutcheon, R.L. McGinnis, A. Achilli, D. Anastasio, A.R. Brady, A.E. Childress, I.V. Farr, N.T. Hancock, J. Lampi, L.D. Nghiem, M. Xie, N.Y. Yip, Standard methodology for evaluating membrane performance in osmotically driven membrane processes, Desalination 312 (2013) 31–38.
[17] J.J. Qin, S. Chen, M.H. Oo, K.A. Kekre, E.R. Cornelissen, C.J. Ruiken, Experimental studies and modeling on concentration polarization in forward osmosis, Water Sci. Technol.—WST 61.11 (2010) 2897–2904.
[18] J.R. McCutcheon, M. Elimelech, Influence of concentrative and dilutive internal concentration polarization on flux behavior in forward osmosis, J. Membr. Sci. 284 (2006) 237–247.
[19] S. Loeb, L. Titelman, E. Korngold, J. Freiman, Effect of porous support fabric on

osmosis through a Loeb-Sourirajan type asymmetric membrane, J. Membr. Sci. 129 (1997) 243–249.
[20] J.R. McCutcheon, R.L. McGinnis, M. Elimelech, Desalination by ammonia–carbon dioxide forward osmosis: influence of draw and feed solution concentrations on process performance, J. Membr. Sci. 278 (2006) 114–123.
[21] J. Koplik, H. Levine, Viscosity renormalization in the Brinkman equation, Phys. Fluids 26 (10) (1983) 2864–2870.
[22] S.S. Manickam, J. Gelb, J.R. McCutcheon, Pore structure characterization of asymmetric membranes: non-destructive characterization of porosity and tortuosity, J. Membr. Sci. 454 (2014) 549–554.
[23] S. Zhang, K.Y. Wang, T.S. Chung, H. Chen, Y.C. Jean, G. Amy, Well-constructed cellulose acetate membranes for forward osmosis: minimized internal concentration polarization with an ultra-thin selective layer, J. Membr. Sci. 360 (2010) 522–535.
[24] M.-F. Paugam, J. Buffle, Comparison of carrier-facilitated copper(II) ion transport mechanisms in a supported liquid membrane and in a plasticized cellulose triacetate membrane, J. Membr. Sci. 147 (1998) 207–215.
[25] J. Wei, C. Qiu, C.Y. Tang, R. Wang, A.G. Fane, Synthesis and characterization of flatsheet thin film composite forward osmosis membranes, J. Membr. Sci. 372 (2011) 292–302.
[26] S. Zhang, K.Y. Wang, T.S. Chung, Y.C. Jean, H. Chen, Molecular design of the cellulose ester-based forward osmosis membranes for desalination, Chem. Eng. Sci. 66 (9) (2011) 2008–2018.
[27] A. Tiraferri, N.Y. Yip, W.A. Phillip, J.D. Schiffman, M. Elimelech, Relating performance of thin-film composite forward osmosis membranes to support layer formation and structure, J. Membr. Sci. 367 (2011) 340–352.